ACS APPLIED ENERGY MATERIALS

www.acsaem.org Article

Mn-Doped Organic–Inorganic Perovskite Nanocrystals for a Flexible Luminescent Solar Concentrator

Sumit S. Bhosale, Efat Jokar, Yi-Ting Chiang, Chieh-Hsi Kuan, Kiana Khodakarami, Zahra Hosseini,* Fang-Chung Chen,* and Eric Wei-Guang Diau*

Cite This: *ACS Appl. Energy Mater.* 2021, 4, 10565–10573 Read Online

ACCESS | Metrics & More | Article Recommendations | Supporting Information

ABSTRACT: We report a robust method of hot addition (HAM) to prepare methylammonium lead trichloride ($MAPbCl_3$) and Mn-doped $MAPbCl_3$ (Mn:$MAPbCl_3$) perovskite nanocrystals (PeNCs) for application in luminescent solar concentrators (LSCs). The HAM, which is free of solvent and operates at high temperatures, is applicable to the synthesis of highly crystalline and stable organic–inorganic PeNCs with tunable optical properties. The Mn:$MAPbCl_3$ PeNCs showed a remarkable energy-transfer shift from 400 to 600 nm that enhanced the optical efficiency when these PeNCs were incorporated in an LSC with a silicon solar-cell module. An optical efficiency (OE) greater than 8% was achieved on incorporation of only 0.094 mass % Mn:$MAPbCl_3$ PeNCs in the LSC. A Monte-Carlo ray-tracing simulation was developed to improve the understanding of the experimental results and estimate the ultimate device performance for future application in building-integrated photovoltaic devices.

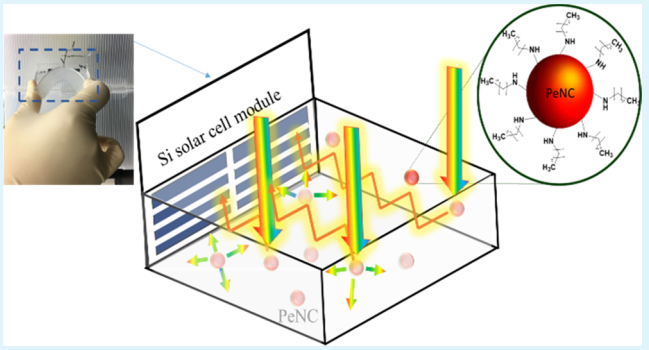

KEYWORDS: *perovskite nanocrystals, hot addition method, luminescent downshifting, optical efficiency, Monte-Carlo ray-tracing simulation*

INTRODUCTION

Apart from bulk halide perovskites that serve as light absorbers for perovskite solar cells,[1−6] perovskite nanocrystals (PeNCs) are materials of interest as emitter centers for lighting applications.[7−9] PeNCs of varied compositions that have been synthesized with diverse methods exhibit varied optical properties, crystallinity, and chemical stability.[10,11] Various synthetic methods such as ligand-assisted reprecipitation (LARP),[12] top-down[13,14] and hot-injection[15] methods have been developed for the synthesis of PeNCs. The LARP method utilizes polar solvents, the residues of which lead to rapid degradation of PeNCs;[16,17] these synthesized PeNCs have poor crystallinity and stability, but researchers subsequently developed modified LARP techniques to stabilize PeNCs.[17,18] The top-down method is an easy way to synthesize PeNCs, but a large distribution of size of PeNCs and a prolonged reaction are drawbacks of this method. The hot-injection method is popular for the synthesis of crystalline all-inorganic PeNCs such as $CsPbX_3$ (X represents a halide ion). In the traditional hot-injection method, only a metal salt (e.g., $PbCl_2$) acts as a halide source, which leads to a halide deficiency in the PeNC structure;[16] the conventional hot-injection method is almost inapplicable for the synthesis of organic–inorganic PeNCs. Moreover, the chemical stability of PeNCs synthesized with this method is a problem to be resolved. When PeNCs are exposed to polar solvents with moisture, they precipitate and change phase, ultimately degrading their optoelectronic performances.[16,17]

Doping of metal cations in PeNCs using cationic species, such as Zn^{2+}, Sn^{2+}, Cd^{2+}, and so on, has been studied;[19] the dopants affect the crystal size, optical properties, and stability of PeNCs. Mn^{2+} is another doping element that has been extensively studied for PeNCs; Mn^{2+} is equivalent to Pb^{2+} and replaces Pb^{2+} in the crystal structure at high temperatures.[20] Mn^{2+}-doped PeNCs exhibit a transfer of exciton energy from the host PeNC to the excited state $^4T_1$ of Mn^{2+}, resulting in a yellow-orange emission.[21] As the transition between the ground state ($^6A_1$) and the excited state of Mn^{2+} is spin-forbidden, it has a negligible absorption coefficient. Mn^{2+} doping has been explored for prospective optical properties and magneto-optical properties.[22] Chloride-based PeNCs provide sufficient energy transfer to excite Mn^{2+} with a dual emission feature at 400 and 600 nm.[21] This large emission

Received: May 26, 2021
Accepted: September 20, 2021
Published: October 4, 2021

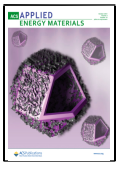

https://doi.org/10.1021/acsaem.1c01498
ACS Appl. Energy Mater. 2021, 4, 10565–10573

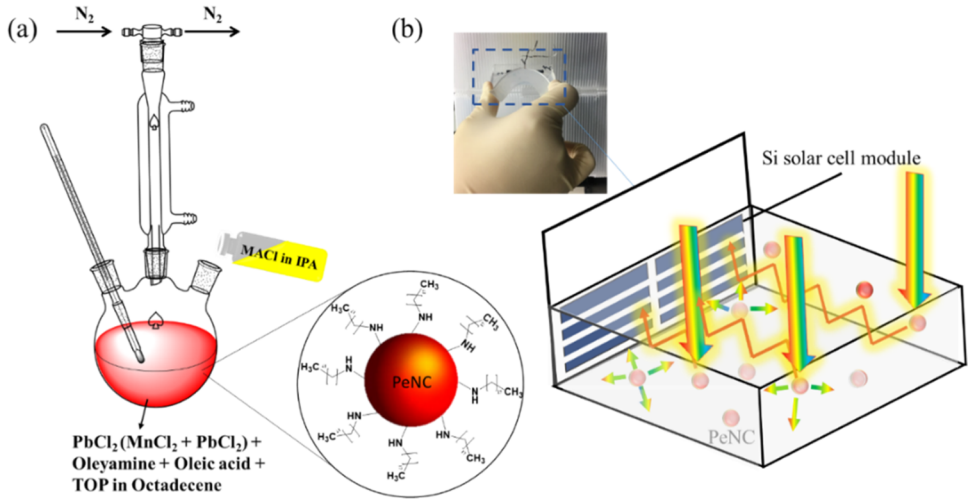

Figure 1. Schematic representation of (a) the method of hot addition for the synthesis of PeNCs and (b) the working mechanism of a luminescent solar concentrator (LSC) and a photograph of a flexible LSC.

band shift from 400 to 600 nm in chloride-based PeNCs makes them suitable candidates for application in a luminescent solar concentrator (LSC).[23] As Mn^{2+} doping in PeNCs requires processing at temperatures 180−260 °C, Mn^{2+} doping in all-inorganic PeNCs has been extensively studied,[24] but little attention has been focused on organic−inorganic PeNCs.

Building-integrated photovoltaic (BIPV) devices has a great appeal for future architectures. LSCs and conventional solar cells can become integrated as photovoltaic windows in urban buildings to generate solar energy. LSCs are made with plastic or glass that is doped or coated with an emissive material;[25] after irradiation with sunlight, luminescent materials emit photons of less energy by downconversion; these photons are guided by total internal reflection toward the solar-cell devices located at the edges of the LSC.[25] Emissive materials of various types, such as organic dyes, polymers, and inorganic semiconductors, have been applied for LSC devices.[26−28] Organometallic materials lack a suitable spectral coverage; the absorption and emission spectra of semiconductor quantum dots and organic dyes overlap.[29]

Here, we report a new method of hot addition (HAM) for the synthesis of hybrid organic−inorganic PeNCs. Even though this method resembles the hot-injection method,[15] it involves a different solvent for the organic cation, and the precursor addition is different (Figure 1a). Organic−inorganic PeNCs synthesized with the hot-injection method require an additional halide precursor to compensate for the halide deficiency in the perovskite structure; also, organic precursor addition is performed at a low temperature (65−100 °C).[30,31] In the HAM, we can synthesize PeNCs at 180−200 °C without the use of an additional halide source, such as an organic salt (e.g., MACl), to decrease the halide deficiency; high-temperature synthesis aids in doping of metal ions in the perovskite nanostructure. We synthesized pristine $MAPbCl_3$ and Mn-doped $MAPbCl_3$ nanocrystals with this method and applied them for LSC application because of the excellent energy-transfer shift of Mn-doped $MAPbCl_3$ that downconverts absorption in the UV region to emission in the visible region, a phenomenon known as luminescent downshifting (LDS). In addition, our LSC has the effect of scattering to enhance the optical efficiency at a larger concentration of PeNCs. Figure 1b shows a schematic working mechanism of the LSC device. A Monte-Carlo ray-tracing (MCRT)[32,33] simulation was performed to provide insight into the role played by PeNCs and to estimate the ultimate performance of devices.

RESULTS AND DISCUSSION

In our HAM approach, $PbCl_2$ was dissolved in 1-octadecene in the presence of trioctylphosphine (TOP); oleyamine and oleic acid acted as protective ligands for PeNCs. After the temperature of the reaction was increased to 200 °C, MACl in 2-propanol (IPA) was added to the clear solution. For the MACl solution, various solvents, such as dimethylformamide, dimethyl sulfoxide, ethanol, and methanol, were tested instead of IPA; although these solvents dissolve MACl easily, they also dissolve PeNCs so as to hinder their formation. IPA is an appropriate solvent for MACl or other organic halide salt and acts as an antisolvent to form PeNCs. Additionally, as IPA has a boiling point of 82.6 °C, it evaporates rapidly at high temperatures. In the HAM, the MACl precursor dissolved in IPA was slowly added into the reactor containing the $PbCl_2$ precursor in 1-octadecene. In contrast, in the hot-injection method, the MACl/IPA precursor must be injected into the reactor at a high temperature (200 °C) so that the IPA rapidly evaporates because of its low boiling point. The needles thereby become blocked by the MACl solid through the rapid evaporation of the IPA solvent using the hot-injection method. Instead of rapid injection, we used a slow addition of a precursor solution to synthesize organic−inorganic PeNCs. After addition of MACl/IPA at 200 °C, the reaction was cooled rapidly to form PeNCs. Our method involves the addition of MACl to a precursor solution at a high temperature (hot addition), which differs from an injection of Cs oleate at a high temperature (hot injection).[15] The hot-injection method is also reported for organic−inorganic PeNCs[30,31] but requires an additional halide precursor. The organic precursor in the hot-injection method was added at 65−100 °C, which was much lower than the temperature that we used in the HAM. According to the literature,[24] for efficient Mn^{2+} doping, a higher temperature (260 °C) is required; the HAM is hence more suitable for synthesizing Mn-doped organic−inorganic PeNCs than the traditional hot-injection method.

Other methods of synthesis of PeNCs were also tested to prove the superiority of our method. We synthesized $MAPbCl_3$

https://doi.org/10.1021/acsaem.1c01498
ACS Appl. Energy Mater. 2021, 4, 10565−10573

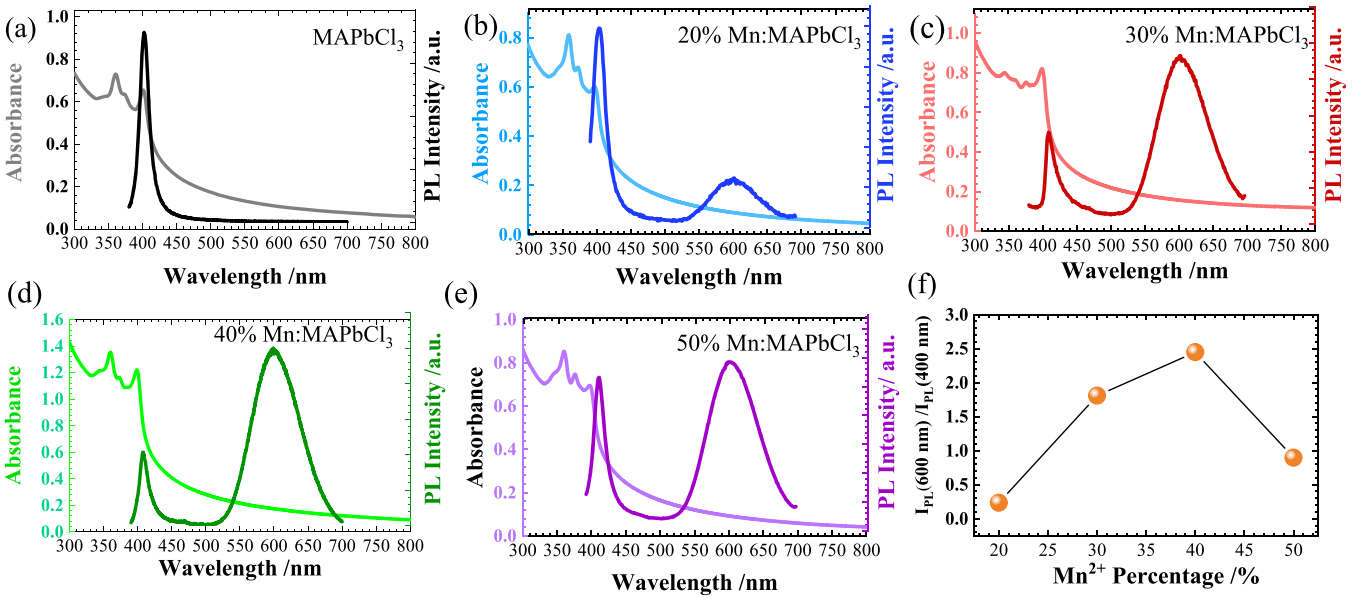

Figure 2. Absorption and emission spectra of (a) $MAPbCl_3$, (b) 20% Mn:$MAPbCl_3$, (c) 30% Mn:$MAPbCl_3$, (d) 40% Mn:$MAPbCl_3$, and (e) 50% Mn:$MAPbCl_3$. (f) PL intensity ratio between 600 and 400 nm for Mn in the $MAPbCl_3$ PeNC in varied proportions.

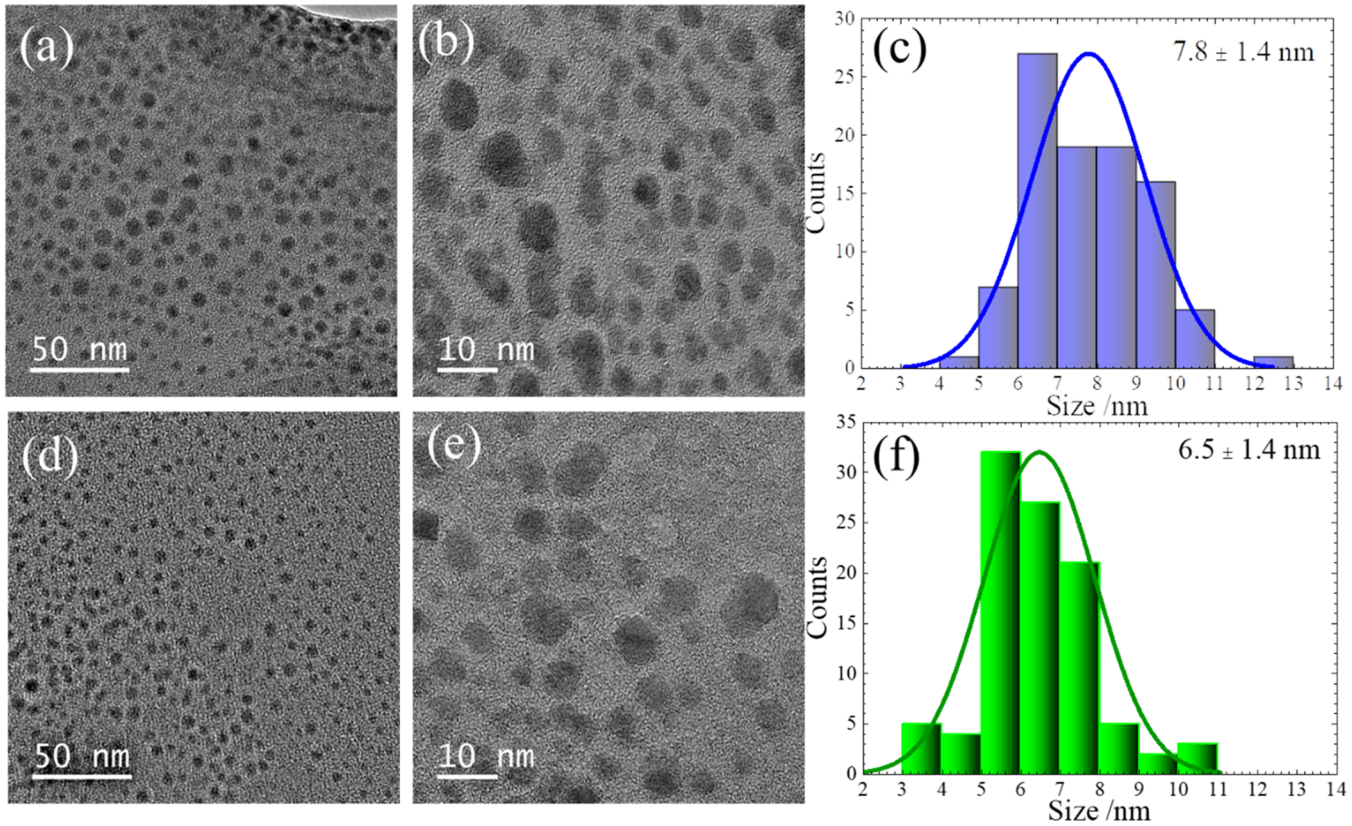

Figure 3. TEM images and size distribution of (a–c) $MAPbCl_3$ and (d–f) 40% Mn-doped $MAPbCl_3$.

with the LARP and top-down methods. Figure S1 shows absorption spectra of PeNCs synthesized differently for storage periods up to 3 weeks. The absorption spectra of PeNCs synthesized with the LAPR and top-down methods clearly show degradation of those samples, whereas the PeNCs synthesized with the HAM are stable. The residual polar solvent remaining after the LARP synthesis is the major issue causing the degradation of PeNCs in the LARP method.[16,17]

The method of hot addition allows us to synthesize highly crystalline and stable organic–inorganic hybrid PeNCs at a high temperature and avoids the use of high boiling-point polar solvents such as dimethylformamide (DMF), dimethyl sulfoxide (DMSO), and *N*-methyl-2-pyrrolidone (NMP); this method is hence ideal for doping metal cations inside PeNCs. For this purpose, Mn^{2+} was doped in $MAPbCl_3$ in varied proportions in molar ratios $MnCl_2/PbCl_2$ of 20, 30, 40, and

https://doi.org/10.1021/acsaem.1c01498
ACS Appl. Energy Mater. 2021, 4, 10565–10573

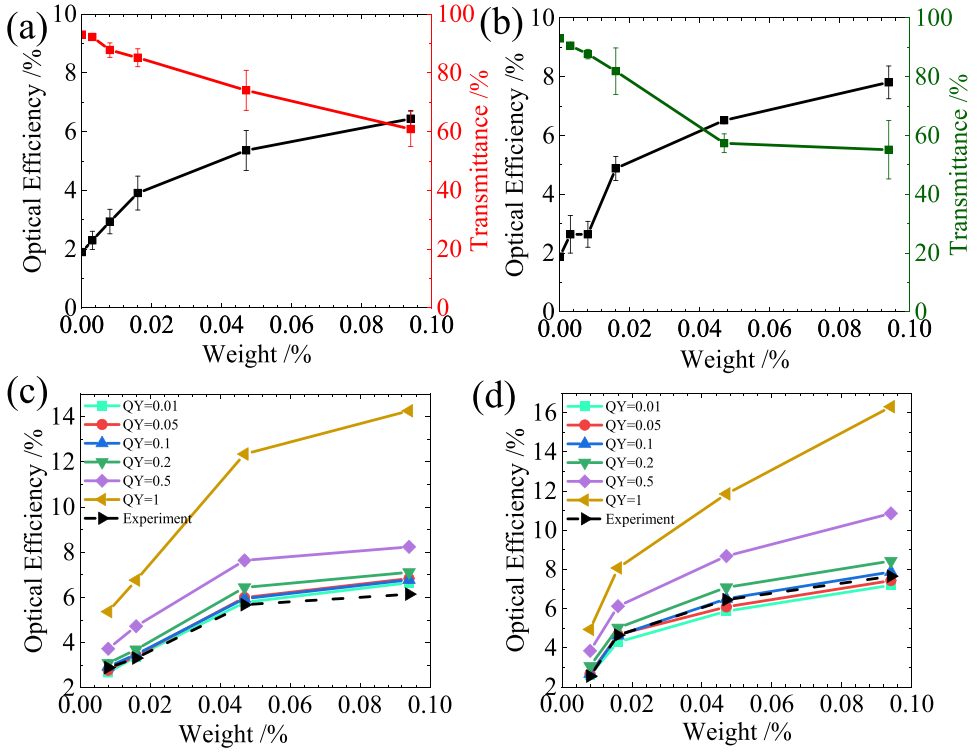

Figure 4. Transmittance (at 600 nm) and optical efficiency vs mass percentage (wt %) of PeNCs in PDMS: (a) PLSC and (b) MnLSC devices and simulation results for (c) PLSC devices and (d) MnLSC devices.

50% in the precursor solution. The absorption spectra show no significant alteration upon doping Mn^{2+} in varied proportions (Figure 2a–e); an excitonic absorption is located at 400 nm. In contrast, the corresponding PL spectra show two specific emissions at 400 and 600 nm with distinct PL intensities (Figure 2f). The emission at ∼400 nm was due to the contribution of pristine excitonic $MAPbCl_3$ PeNCs, but a further emission at ∼600 nm appeared when Mn^{2+} was doped inside the $MAPbCl_3$ PeNC. The observed PL at 600 nm is assigned to a forbidden transition $^4T_1 \rightarrow {}^6A_1$ of cation Mn^{2+}.[21] On increasing the proportion of $MnCl_2$, we observed that the PL intensity at 400 nm decreased, whereas that at 600 nm increased. At 600 nm, photoluminescence quantum yields (PLQYs) with 2.3, 3.5, 4.0, and 5.9% were obtained for 20, 30, 40, and 50% Mn doping, respectively. The ratio of the PL intensity at 600 nm to that at 400 nm increased for $MnCl_2$/$PbCl_2$ ratio from 20 to 40% because of an enhanced energy transfer from the host ($MAPbCl_3$) to the dopant (Mn^{2+}), but it decreased at 50% (Figure 2e,f) because of the enhanced Mn–Mn interaction that quenched the emission of Mn^{2+}.[34,35] The best condition for the downconversion of solar energy from 400 to 600 nm occurred for the Mn:$MAPbCl_3$ PeNC with the ratio $MnCl_2/PbCl_2$ of 40%, which exhibits a photoluminescence quantum yield of 4% at 600 nm; we thus used that PeNC for our LSC application.

Other than the HAM, Mn:$MAPbCl_3$ PeNCs can be synthesized with the LARP method. We synthesized 40% Mn-doped PeNCs according to the LARP procedure;[36] the corresponding PL spectrum is shown in Figure S2a. The stability of Mn-doped PeNCs fabricated with the LARP method is, however, poor compared with Mn-doped PeNCs from the HAM (Figure S2b,c). Mn-doped PeNCs cannot be produced using the top-down method.

Powder X-ray diffraction (XRD) patterns of thin-film PeNC samples are shown in Figure S3. These patterns of $MAPbCl_3$ and 40% Mn:$MAPbCl_3$ are similar, with a cubic crystal structure *Pm*3*m*.[36,37] The diffraction signals of both samples are slightly shifted with respect to the standard crystallographic data, which is attributed to the nanocrystalline nature of these samples.[38] No shift of XRD patterns was observed for the 40% Mn-doped sample compared to the standard undoped PeNC sample, indicating that the proportion of Mn^{2+} in PeNCs is small. To determine that proportion, we recorded an inductively coupled plasma optical-emission spectrum (ICP-OES); the results are listed in Table S1. Even though $MnCl_2$ at 40% with respect to $PbCl_2$ was added to the precursor solution, Mn^{2+} at only 0.021% was found inside the host PeNC. This minute proportion of Mn^{2+} dopant in $MAPbCl_3$ PeNCs plays a key role in the crystallinity (Figure S3) and size of the PeNCs. Figure 3 shows images from a transmission electron microscope (TEM) under varied magnifications. Figure S4 shows HRTEM images of PeNCs; interplanar distances of 0.25 nm in $MAPbCl_3$ and 0.32 nm in Mn-$MAPBcl_3$ are assigned to the (210) and (111) planes of a cubic phase, respectively. The average sizes of the two PeNCs are 7.8 ± 1.4 nm for $MAPbCl_3$ and 6.5 ± 1.4 nm for 40% Mn:$MAPbCl_3$. The latter smaller size is attributed to the Mn-doping effect according to which a small portion of the Pb^{2+} vacancies are replaced by the Mn^{2+} species.[39,40]

As mentioned above, the large energy-transfer shift of Mn:$MAPbCl_3$ avoids the self-reabsorption of PL emission by PeNCs and makes them suitable as emissive centers in LSCs.[23] To fabricate a flexible LSC, we used soft poly(dimethylsiloxane) (PDMS) as a polymer base that is transparent in the solar spectrum;[41] PeNCs were dispersed in the polymer slab. We followed a typical design for the LSC in which the silicon solar cell (SSC) was submerged in the

https://doi.org/10.1021/acsaem.1c01498
ACS Appl. Energy Mater. 2021, 4, 10565–10573

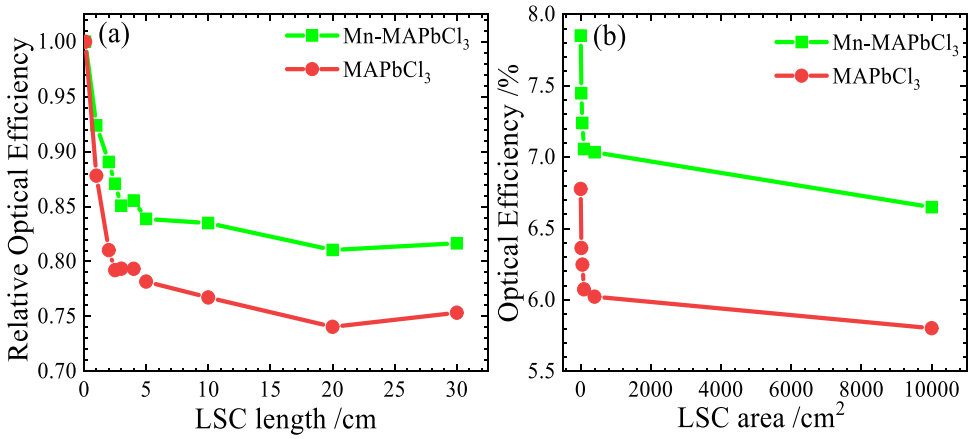

Figure 5. Simulated data: (a) relative optical efficiency vs LSC length and (b) optical efficiency vs LSC area.

polymer and attached onto one side of the LSC (Figure 1b). To test the effect of Mn:$MAPbCl_3$ in LSCs, LSCs of dimensions 2.8 × 2.5 × 1.4 cm^3 (G factor ∼ 5.0) were fabricated according to three experimental conditions: (i) an LSC fabricated with only PDMS (BLSC), (ii) an LSC fabricated with pristine $MAPbCl_3$, which has photoluminescence quantum yield of 0.7% (PLSC), and (iii) an LSC fabricated with 40% Mn-doped $MAPbCl_3$ (MnLSC). In the second and third conditions, LSCs in a series with varied proportions of PeNCs inside PDMS were prepared to study the effect of mass percentage (mass %) on the LSC performance. As shown in Figure S5, the transmittance of the LSC decreased and the corresponding PL intensity increased on increasing the proportions of PeNCs. A current−voltage curve and an IPCE spectrum of a commercial silicon solar cell under one-sun irradiation are displayed in Figure S6. Figure S7a,b shows the current−voltage curves of the PLSC and MnLSC devices, respectively, under one-sun irradiation; the actual LSC device is shown in Figure S8. The corresponding photovoltaic results are summarized in Tables S2 and S3 for the PLSC and MnLSC devices, respectively. For both PLSC and MnLSC devices, the values of the short-circuit photocurrent (I_{sc}) increased upon increasing the mass % of the PeNCs inside LSCs, whereas the transmittances of the devices decreased. At small mass %, V_{oc} decreased as the number of photons reaching the solar cell decreased because of a smaller contribution from LDS and scattering.[42]

The enhanced I_{sc} of MnLSC devices is due to the effects of both light scattering and luminescent downshifting, whereas that of the PLSC devices is due to only the scattering effect. The irradiated areas of the device were also considered. We define the optical efficiency (OE) as OE = I_{sc} (LSC) × A_{SSC}/I_{sc} (SSC) × A_{LSC}, where I_{sc} (SSC) are photocurrents generated by LSC and SSC devices, and A_{SSC} and A_{LSC} are areas of SSC and LSC, respectively.[43] The OE values of the PLSC and MnLSC devices are listed in Tables S2 and S3, respectively.

Although increasing the proportion of PeNCs in the LSC enhances the optical efficiency of the devices, the transmittance of the LSC decreases. Figure 4a,b shows the transmittance and optical efficiency vs concentration of PeNCs for the PLSC and MnLSC devices, respectively. The results indicate that, even though the same proportions of PeNCs were present in the LSCs, the MnLSC device has a lower transmittance than the PLSC device. This effect is attributed to the varied sizes of Mn-doped PeNCs and pristine PeNCs. As shown in Figure 3, as the Mn-doped PeNCs were much smaller than the pristine PeNCs; the number of Mn-doped PeNCs would be much greater than that of the pristine PeNCs. The effect of scattering hence became much greater for the former than for the latter; this effect caused a rapid decrease of the transmittance upon increasing the PeNC concentrations in the MnLSC devices. The small transmittance with a large PeNC concentration is inapplicable for photovoltaic windows even though the obtained optical efficiency is large. These LSCs are most suitable for applications such as integrated wearable devices or clothing-integrated photovoltaics. Both curves of transmittance and optical efficiency have a crossing point at transmittance 60−70% and optical efficiency ∼6%, for which the optimal PeNC amounts are ∼0.09 and ∼0.04 mass % for PLSC and MnLSC, respectively.

An MCRT simulation of light propagation in LSCs filled with $MAPbCl_3$ and Mn:$MAPbCl_3$ PeNCs was undertaken based on the experimental absorption and PL spectra in Figure 2. The MCRT model was used to calculate the OE of the LSCs containing $MAPbCl_3$ and Mn:$MAPbCl_3$ PeNCs at varied mass percentages. For each LSC, the OE vs PeNC concentration was investigated for varied luminescent quantum yields (QYs). The experimental and MCRT-simulated OE values are shown in Figure 4c,d for PLSC and MnLSC, respectively; the calculated OE of MnLSC agrees satisfactorily with the experimental results for a luminescent QY of less than 10%. The simulation results show that the OE obtained for each LSC is due to not only the effect of luminescent downshifting but also the effect of scattering of incident photons in the LSC. The extent of contributions of LDS and scattering effects to OE are listed in Tables S4 and S5 for PLSC and MnLSC, respectively. Although the scattering effect decreased the transparency of the LSC, it guided photons toward the solar cell and increased the number of photons reaching that cell. There are reports in the literature on inducing a scattering effect of the LSC either by adding scatterer particles to the LSC or by painting white the back plate of the LSC,[41,44,45] but our Mn-doped PeNCs showed a dual-functionality to have a scattering-enhanced LSC device.

Light absorption by the LSC increased on increasing the PeNC proportion. Enhanced light absorption by PeNCs in the LSC led to an increased number of downshifted photons, thereby an increased OE of the LSC. Comparing Figure 4c,d, one sees that, when using $MAPbCl_3$ PeNCs, the change in OE as a function of concentration occurred more smoothly. This

https://doi.org/10.1021/acsaem.1c01498
ACS Appl. Energy Mater. 2021, 4, 10565−10573

effect is attributed to the greater reabsorption in the LSC containing $MAPbCl_3$ PeNCs compared to the LSC containing Mn:$MAPbCl_3$ PeNCs. We quantified the reabsorption with a parameter radiative overlap (RO). The RO values for PLSC and MnLSC at varied weight percentages are tabulated in Table S6. At a concentration of 0.094 mass %, RO was 0.89 for PLSC and 0.23 for MnLSC. When the RO was large, although light absorption increased on increasing the PeNC proportion in the LSC, the chance of reabsorption of the emitted photons was also large. The OE hence did not increase substantially on increasing the PeNC amount; this behavior was pronounced in cases of small QY. As a result, the QY determined the extent of the negative effect of RO on the performance of the LSC. When the QY was small, the chance to contribute to the OE via the reabsorbed photons was small and the loss due to RO was considerable and vice versa; the larger the QY, the smaller the RO loss.

To estimate the ultimate device performances achievable using $MAPbCl_3$ and Mn:$MAPbCl_3$ PeNCs, we also simulated the LSC OE in varied LSC sizes. In the calculation of the following results, the concentration and QY were fixed at 0.09 mass % and 0.1, respectively, for both $MAPbCl_3$ and Mn:$MAPbCl_3$ PeNCs.

Figures 5a and S9a show plots of the relative OE calculated using MCRT simulations with increasing LSC length (from 0.1 to 30 cm) and *G* factor (from 0 to 55), respectively, for PLSC and MnLSC devices. The width and thickness (height) of LSCs were fixed at the experimental values in these calculations. As expected, the OE decreased exponentially with increasing LSC length because of the combined effects of reabsorption loss and escape loss. The total OE of MnLSC and PLSC decreased by 16 and 22%, respectively, at length ~5 cm and then remained almost unchanged for MnLSC with greater lengths. A larger decrease of OE of PLSC compared with that of MnLSC is attributed to the effect of RO. For the LSC with a greater RO, the chance of reabsorption of emitted photons increased on increasing the photon path caused by increased LSC length. In a longer LSC, the chance of photon escape due to scattering is also greater. The OE hence decreased on increasing the LSC length. The simulation results show, however, that the OE of the MnLSC device does not decrease more than 20% even for a long LSC. Figures 5b and S9b show the calculated OE for MnLSC and PLSC devices with varying areas and *G* factors, respectively. In general, as the area of the top surface of the LSCs increased, more photons entered the LSC but had a greater chance of being lost through reabsorption or escape of photons. For a fixed LSC thickness, the simulation results thus show a decreased OE on increasing the LSC area from about 2.5×2.5 cm^2 to 100×100 cm^2. The amount of decrease of LSC OE is about 14−15% for both PLSC and MnLSC devices. Table S7 shows that both the LDS share and scattering share decreased on increasing the LSC area, which is attributed to the effects of greater reabsorption and photon escape, respectively.

The stability of an LSC is an important factor to consider for its commercial applications. Stability tests of both PLSC and MnLSC devices were undertaken to address this issue. The stability of Mn:$MAPbCl_3$ nanocrystals was analyzed by monitoring the PL intensity of a sample for 1 month. Figure S10 shows excellent stability of the PeNC synthesized with the HAM; only a slight change was observed in the PL spectrum after the sample was stored in darkness for 1 month. The slight red shift in PL at 400 nm for the aged solution is related to the progressive release of Mn^{2+} from the host structure.[20] Moreover, the performance stabilities of the PLSC and MnLSC devices were analyzed when they were stored in darkness under ambient conditions for 3 months (Figure S11). Because the perovskite nanocrystals in PDMS are not evenly distributed, a slight change in the LSC position alters the light scattering, thus reflecting the fluctuation of the stability data. The great stability of LSCs is attributed to the robust silicone backbone of the PDMS enclosing the PeNCs. We thus provide strong evidence for the excellent stability of both PLSC and MnLSC devices with PeNCs synthesized with the HAM. MnLSC at a concentration of 0.094% was tested for the flexibility study because PDMS is flexible with excellent mechanical properties. Two cylinders were used to bend the LSC with bending radii 9 and 15 mm. The current−voltage curves shown in Figure S12; the corresponding photovoltaic parameters are listed in Table S8. The results show that both 15- and 9-mm bending devices have poorer photocurrents and efficiencies of power conversion than those of the flat device because, on bending, the photocurrent decreases as the path length of light reaching the solar cell increases.[46]

CONCLUSIONS

We developed a novel method of hot addition to prepare organic−inorganic perovskite nanocrystals ($MAPbCl_3$ and Mn-doped $MAPbCl_3$). The stability of PeNCs made with our HAM is better than that with other commonly used synthetic methods (LARP or top-down methods). Doping of Mn^{2+} cations in $MAPbCl_3$ induces a luminescent downshifting (LDS) effect with a significant energy-transfer shift from 400 to 600 nm that avoids reabsorption of the emitted photons and makes them suitable for application in an LSC. On application of PeNCs as emitter centers in the LSC, a greater optical efficiency for the MnLSC relative to the PLSC at the same mass percentage of PeNCs is achieved, which is attributed to a smaller RO between the absorption and emission of the Mn-doped $MAPbCl_3$ nanocrystals. A Monte-Carlo ray-tracing simulation confirmed the experimental observations of the enhanced optical efficiency of the MnLSC device. We hence demonstrated the feasiblity of synthesis of stable Mn-doped $MAPbCl_3$ PeNCs with the HAM and used them to enhance the light-harvesting ability and serve as a potential candidate for a luminescent solar concentrator.

EXPERIMENTAL SECTION

Materials. All materials were used without purification: lead chloride ($PbCl_2$, 99%, Sigma-Aldrich), methylammonium chloride (MACl, 99%, Sigma-Aldrich), manganese chloride ($MnCl_2$, 99%, Sigma-Aldrich), oleylamine (OLA, technical grade, 70%, Sigma-Aldrich), oleic acid (OA, technical grade, 90%, Sigma-Aldrich), trioctylphosphine (TOP, anhydrous, 90%, Sigma-Aldrich), anhydrous 2-propanol and toluene (99.5%, Sigma-Aldrich), and Sylgard 184 silicone elastomer kit (Dow Chemical).

Synthesis of Perovskite Nanocrystals. *Method of Hot Addition.* Perovskite nanocrystals (PeNCs) were synthesized with the method of hot addition. $PbCl_2$ (0.94 mmol) and TOP (5 mL) were placed with 1-octadecene (25 mL) in a spherical flask; the mixture was heated at 100 °C under vacuum for 1 h. MACl (0.94 mmol) was placed in a bottle (5 mL) to which IPA (3 mL) was added. The mixture was heated to dissolve MACl in IPA resulting in a clear solution. After heating $PbCl_2$ in octadecene for 1 h, OLA and OA (2.5 mL) were added; the temperature was increased to 200 °C. MACl in IPA was added slowly to the clear solution; the solution was cooled with an ice bath. For Mn doping, a molar percentage of $MnCl_2$ varied with respect to $PbCl_2$ was added in TOP and 1-octadecene.

https://doi.org/10.1021/acsaem.1c01498
ACS Appl. Energy Mater. 2021, 4, 10565−10573

The procedures such as applying vacuum, heating, and precursor addition were the same as those for undoped PeNCs. To purify the PeNCs, the crude solution was centrifuged at 9500 rpm for 40 min; the precipitate was washed with toluene. This washed precipitate was dispersed in toluene.

Ligand-Assisted Reprecipitation. $CH_3NH_3PbCl_3$ PeNCs were prepared according to a reported procedure.[36] A precursor solution (1.5 mL) of PeNCs was prepared by dissolving MACl (0.05 mmol), $PbCl_2$ (0.05 mmol), oleylamine (40 μL), and oleic acid (40 μL) in DMF (1.5 mL); the mixture was ultrasonicated until the solution became transparent. The precursor solution (100 μL) was injected into toluene (5 mL) to form a suspension of $MAPbCl_3$ PeNCs. Mn^{2+}-doped $MAPbCl_3$ PeNCs were prepared by adding $MnCl_2$ at a molar ratio of 40% with respect to $PbCl_2$ to the precursor solution. The remaining procedure was the same as that for the LARP method used for the $MAPbCl_3$ PeNC synthesis.

Top-Down Method. The top-down method was implemented according to a previous report.[13] $PbCl_2$ (0.8 mmol) and MACl were placed in a falcon tube. Oleic acid (40 mL) and oleylamine (4 mL) were added to this mixture, which was sealed and sonicated (Elmasonic Easy 120 H, frequency 50−60 Hz) for 3−5 days. During sonication, bulk perovskite crystals were formed, which fragmented into nanocrystals; these nanocrystals were protected with capping ligands. After sonication, the reaction mixture was centrifuged at 2000 rpm for 10 min to remove large particles and then centrifuged at 9500 rpm for 40 min to extract the fine nanocrystals. The precipitate was dispersed in toluene and again centrifuged to wash the excess capping ligand. The final precipitate was redispersed in toluene.

Fabrication of the LSC. The LSC was fabricated using a PDMS polymer.[41] For a blank LSC, silicon elastomer A (13.0 g) and silicon elastomer B (1.3 g) were mixed; the mixture was kept under vacuum for 1 h to remove air bubbles. After 1 h, the mixture was poured into a polyacrylic mold, in which a silicon solar cell was placed at the edge. This assembly was heated at 70 °C for 60 min; after heating, the solidified LSC device was peeled from the mold. For the fabrication of PLSC and MnLSC, PeNCs with amounts 0.45 (0.003 mass %), 1.12 (0.008 mass %), 2.25 (0.016 mass %), 6.75 (0.047 mass %), and 13.5 (0.094 mass %) mg suspended in toluene were mixed in the silicon elastomer mixture and then poured into the mold. The PeNC and PDMS mixture was kept under vacuum to remove air bubbles and the solvent toluene. After application of vacuum, the mold was transferred to an oven and heated at 70 °C for 60 min; the solidified LSC device was then peeled from the mold.

ICP-OES Sample Preparation. The nanocrystal solution was evaporated; a nanocrystal powder was collected. This powder was dissolved in aqua regia (2 mL, HCl/HNO_3 = 3:1). The digested PeNC solution was diluted with distilled water to 20 mL. Before characterization, the diluted solution was centrifuged to remove undigested materials.

Characterization. X-ray diffraction (XRD) patterns of PeNCs coated on indium tin oxide (ITO) substrates were obtained with an X-ray diffractometer (Bruker AXS, D8 Advance, Cu Kα irradiation, λ = 154.18 pm). Absorption spectra for PeNCs were recorded in the range 300−800 nm (V-780 JASCO), and photoluminescence (PL) spectra were recorded in the range 380−700 nm (excitation at 350 nm, LDH-635, PicoQuant). The current density−voltage characteristics of devices were recorded with a digital source meter (Keithley 2400) under one-sun illumination (AM 1.5G, 100 mW cm^{-2}) with a solar simulator (XES-40S1, SAN-E1) and calibrated with a silicon diode and a KG-5 filter to decrease the mismatch of the spectrum. The spectra of incident photons to current (IPCE) were recorded with a system comprising a Xe lamp (A-1010, PTi, 150 W) and a monochromator (PTi). The amount of Mn in PeNCs was determined with an inductively coupled plasma optical-emission spectrometer (Varian 720 ES).

Monte-Carlo Simulations. For 3D Monte-Carlo simulations, we used the model of a box-shaped LSC, with experimental dimensions, unless otherwise stated. The top surface pointed toward the sun; one side was covered with a solar cell and the other sides were attached to perfectly reflecting mirrors; and the bottom surface was clear. The normally incident radiation was sampled from the solar spectrum and 10^5 photons were traced in each simulation. Propagation distances inside the LSC were based on inverting the Beer−Lambert law using measured absorbance and transmission spectra. Photons absorbed by the luminescent species inside the LSC were considered to be emitted isotropically. Photons striking the top or bottom surface were probabilistically reflected or transmitted based on Snell's law of reflection with PDMS host refractive index n = 1.43. Photons were monitored until they struck the side at which they would be collected by the solar cell, escaped through the top or bottom surface, or were lost by nonradiative routes and thus not re-emitted. The scattering of photons by PeNCs in the LSC was also considered in all simulations based on the transmission spectrum.

■ ASSOCIATED CONTENT

Supporting Information

The Supporting Information is available free of charge at https://pubs.acs.org/doi/10.1021/acsaem.1c01498.

Absorption and photoluminescence spectra of perovskite nanocrystals synthesized with various methods, TEM images and XRD patterns of perovskite nanocrystals, photographs of LSC devices, stability, and current, and voltage plots of LSC devices (PDF)

■ AUTHOR INFORMATION

Corresponding Authors

Zahra Hosseini − *Faculty of Advanced Technologies, Shiraz University, 7194684560 Shiraz, Iran*; Email: zahrahosseini@shirazu.ac.ir

Fang-Chung Chen − *Department of Photonics, Institute of EO Engineering of Display, Hsinchu 30010, Taiwan*; Email: fcchen@mail.nctu.edu.tw

Eric Wei-Guang Diau − *Department of Applied Chemistry and Institute of Molecular Science, National Yang Ming Chiao Tung University, Hsinchu 30010, Taiwan; Center for Emergent Functional Matter Science, National Yang Ming Chiao Tung University, Hsinchu 30010, Taiwan*; orcid.org/0000-0001-6113-5679; Email: diau@mail.nctu.edu.tw

Authors

Sumit S. Bhosale − *Department of Applied Chemistry and Institute of Molecular Science, National Yang Ming Chiao Tung University, Hsinchu 30010, Taiwan*

Efat Jokar − *Department of Applied Chemistry and Institute of Molecular Science, National Yang Ming Chiao Tung University, Hsinchu 30010, Taiwan; Center for Emergent Functional Matter Science, National Yang Ming Chiao Tung University, Hsinchu 30010, Taiwan*

Yi-Ting Chiang − *Department of Applied Chemistry and Institute of Molecular Science, National Yang Ming Chiao Tung University, Hsinchu 30010, Taiwan*

Chieh-Hsi Kuan − *Department of Applied Chemistry and Institute of Molecular Science, National Yang Ming Chiao Tung University, Hsinchu 30010, Taiwan*

Kiana Khodakarami − *Faculty of Advanced Technologies, Shiraz University, 7194684560 Shiraz, Iran*

Complete contact information is available at: https://pubs.acs.org/10.1021/acsaem.1c01498

Notes

The authors declare no competing financial interest.

https://doi.org/10.1021/acsaem.1c01498
ACS Appl. Energy Mater. 2021, 4, 10565−10573

■ ACKNOWLEDGMENTS

Taiwan Ministry of Science and Technology (MOST 110-2123-M-A49-001 and MOST 110-2634-F-009-026) and Center for Emergent Functional Matter Science of National Yang Ming Chiao Tung University (NYMCTU) from the Featured Areas Research Center Program within the framework of the Higher Education Sprout Project by Taiwan Ministry of Education (MOE) supported this research.

■ REFERENCES

(1) Jokar, E.; Chien, C.-H.; Tsai, C.-M.; Fathi, A.; Diau, E. W.-G. Robust Tin-Based Perovskite Solar Cells with Hybrid Organic Cations to Attain Efficiency Approaching 10%. *Adv. Mater.* **2019**, *31*, No. 1804835.

(2) Yang, W. S.; Park, B.-W.; Jung, E. H.; Jeon, N. J.; Kim, Y. C.; Lee, D. U.; Shin, S. S.; Seo, J.; Kim, E. K.; Noh, J. H.; Seok, S. Il. Iodide Management in Formamidinium-Lead-Halide−Based Perovskite Layers for Efficient Solar Cells. *Science* **2017**, *356*, 1376−1379.

(3) Bhosale, S. S.; Jokar, E.; Fathi, A.; Tsai, C.-M.; Wang, C.-Y.; Diau, E. W.-G. Functionalization of Graphene Oxide Films with Au and MoO_x Nanoparticles as Efficient p -Contact Electrodes for Inverted Planar Perovskite Solar Cells. *Adv. Funct. Mater.* **2018**, *28*, No. 1803200.

(4) Jokar, E.; Chien, C.-H.; Fathi, A.; Rameez, M.; Chang, Y.-H.; Diau, E. W.-G. Slow Surface Passivation and Crystal Relaxation with Additives to Improve Device Performance and Durability for Tin-Based Perovskite Solar Cells. *Energy Environ. Sci.* **2018**, *11*, 2353−2362.

(5) Jiang, X.; Wang, F.; Wei, Q.; Li, H.; Shang, Y.; Zhou, W.; Wang, C.; Cheng, P.; Chen, Q.; Chen, L.; Ning, Z. Ultra-High Open-Circuit Voltage of Tin Perovskite Solar Cells via an Electron Transporting Layer Design. *Nat. Commun.* **2020**, *11*, No. 1245.

(6) Shahbazi, S.; Li, M.; Fathi, A.; Diau, E. W. Realizing a Cosolvent System for Stable Tin-Based Perovskite Solar Cells Using a Two-Step Deposition Approach. *ACS Energy Lett.* **2020**, *5*, 2508−2511.

(7) Jeon, S.; Lee, S. Y.; Kim, S.; Kim, W.; Park, T.; Bang, J.; Ahn, J.; Woo, H. K.; Chae, J.; Paik, T.; Seong, T.; Oh, S. J. All-Solution Processed Multicolor Patterning Technique of Perovskite Nanocrystal for Color Pixel Array and Flexible Optoelectronic Devices. *Adv. Opt. Mater.* **2020**, *8*, No. 2000501.

(8) Zheng, X.; Yuan, S.; Liu, J.; Yin, J.; Yuan, F.; Shen, W.-S.; Yao, K.; Wei, M.; Zhou, C.; Song, K.; Zhang, B.-B.; Lin, Y.; Hedhili, M. N.; Wehbe, N.; Han, Y.; Sun, H.-T.; Lu, Z.-H.; Anthopoulos, T. D.; Mohammed, O. F.; Sargent, E. H.; Liao, L.-S.; Bakr, O. M. Chlorine Vacancy Passivation in Mixed Halide Perovskite Quantum Dots by Organic Pseudohalides Enables Efficient Rec. 2020 Blue Light-Emitting Diodes. *ACS Energy Lett.* **2020**, *5*, 793−798.

(9) Zhang, X.; Gao, L.; Zhao, M.; Miao, Y.; Wang, Z.; Wang, C.; Liu, P.; Xu, B.; Guo, J. Low-Temperature Direct Synthesis of Perovskite Nanocrystals in Water and Their Application in Light-Emitting Diodes. *Nanoscale* **2020**, *12*, 6522−6528.

(10) Zhang, Y.; Liu, J.; Wang, Z.; Xue, Y.; Ou, Q.; Polavarapu, L.; Zheng, J.; Qi, X.; Bao, Q. Synthesis, Properties, and Optical Applications of Low-Dimensional Perovskites. *Chem. Commun.* **2016**, *52*, 13637−13655.

(11) Huang, H.; Polavarapu, L.; Sichert, J. A.; Susha, A. S.; Urban, A. S.; Rogach, A. L. Colloidal Lead Halide Perovskite Nanocrystals: Synthesis, Optical Properties and Applications. *NPG Asia Mater.* **2016**, *8*, e328.

(12) Schmidt, L. C.; Pertegás, A.; González-Carrero, S.; Malinkiewicz, O.; Agouram, S.; Mínguez Espallargas, G.; Bolink, H. J.; Galian, R. E.; Pérez-Prieto, J. Nontemplate Synthesis of $CH_3NH_3PbBr_3$ Perovskite Nanoparticles. *J. Am. Chem. Soc.* **2014**, *136*, 850−853.

(13) Huang, H.; Xue, Q.; Chen, B.; Xiong, Y.; Schneider, J.; Zhi, C.; Zhong, H.; Rogach, A. L. Top-Down Fabrication of Stable Methylammonium Lead Halide Perovskite Nanocrystals by Employing a Mixture of Ligands as Coordinating Solvents. *Angew. Chem., Int. Ed.* **2017**, *56*, 9571−9576.

(14) Bhosale, S. S.; Kharade, A. K.; Jokar, E.; Fathi, A.; Chang, S.; Diau, E. W.-G. Mechanism of Photocatalytic CO_2 Reduction by Bismuth-Based Perovskite Nanocrystals at the Gas−Solid Interface. *J. Am. Chem. Soc.* **2019**, *141*, 20434−20442.

(15) Protesescu, L.; Yakunin, S.; Bodnarchuk, M. I.; Krieg, F.; Caputo, R.; Hendon, C. H.; Yang, R. X.; Walsh, A.; Kovalenko, M. V. Nanocrystals of Cesium Lead Halide Perovskites ($CsPbX_3$, X = Cl, Br, and I): Novel Optoelectronic Materials Showing Bright Emission with Wide Color Gamut. *Nano Lett.* **2015**, *15*, 3692−3696.

(16) Shamsi, J.; Urban, A. S.; Imran, M.; De Trizio, L.; Manna, L. Metal Halide Perovskite Nanocrystals: Synthesis, Post-Synthesis Modifications, and Their Optical Properties. *Chem. Rev.* **2019**, *119*, 3296−3348.

(17) Zhang, F.; Huang, S.; Wang, P.; Chen, X.; Zhao, S.; Dong, Y.; Zhong, H. Colloidal Synthesis of Air-Stable $CH_3NH_3PbI_3$ Quantum Dots by Gaining Chemical Insight into the Solvent Effects. *Chem. Mater.* **2017**, *29*, 3793−3799.

(18) Gonzalez-Carrero, S.; Francés-Soriano, L.; González-Béjar, M.; Agouram, S.; Galian, R. E.; Pérez-Prieto, J. The Luminescence of $CH_3NH_3PbBr_3$ Perovskite Nanoparticles Crests the Summit and Their Photostability under Wet Conditions Is Enhanced. *Small* **2016**, *12*, 5245−5250.

(19) van der Stam, W.; Geuchies, J. J.; Altantzis, T.; van den Bos, K. H. W.; Meeldijk, J. D.; Van Aert, S.; Bals, S.; Vanmaekelbergh, D.; de Mello Donega, C. Highly Emissive Divalent-Ion-Doped Colloidal $CsPb_{1-x}M_x$ Br_3 Perovskite Nanocrystals through Cation Exchange. *J. Am. Chem. Soc.* **2017**, *139*, 4087−4097.

(20) Chen, D.; Fang, G.; Chen, X.; Lei, L.; Zhong, J.; Mao, Q.; Zhou, S.; Li, J. Mn-Doped $CsPbCl_3$ Perovskite Nanocrystals: Solvothermal Synthesis, Dual-Color Luminescence and Improved Stability. *J. Mater. Chem. C* **2018**, *6*, 8990−8998.

(21) Liu, W.; Lin, Q.; Li, H.; Wu, K.; Robel, I.; Pietryga, J. M.; Klimov, V. I. Mn^{2+}-Doped Lead Halide Perovskite Nanocrystals with Dual-Color Emission Controlled by Halide Content. *J. Am. Chem. Soc.* **2016**, *138*, 14954−14961.

(22) Das Adhikari, S.; Dutta, A.; Dutta, S. K.; Pradhan, N. Layered Perovskites $L_2(Pb_{1-x}Mn_x)Cl_4$ to Mn-Doped $CsPbCl_3$ Perovskite Platelets. *ACS Energy Lett.* **2018**, *3*, 1247−1253.

(23) Meinardi, F.; Akkerman, Q. A.; Bruni, F.; Park, S.; Mauri, M.; Dang, Z.; Manna, L.; Brovelli, S. Doped Halide Perovskite Nanocrystals for Reabsorption-Free Luminescent Solar Concentrators. *ACS Energy Lett.* **2017**, *2*, 2368−2377.

(24) Pradhan, N. Tips and Twists in Making High Photoluminescence Quantum Yield Perovskite Nanocrystals. *ACS Energy Lett.* **2019**, *4*, 1634−1638.

(25) Zhou, Y.; Zhao, H.; Ma, D.; Rosei, F. Harnessing the Properties of Colloidal Quantum Dots in Luminescent Solar Concentrators. *Chem. Soc. Rev.* **2018**, *47*, 5866−5890.

(26) Huang, C.-S.; Jakubowski, K.; Ulrich, S.; Yakunin, S.; Clerc, M.; Toncelli, C.; Rossi, R. M.; Kovalenko, M. V.; Boesel, L. F. Nano-Domains Assisted Energy Transfer in Amphiphilic Polymer Conetworks for Wearable Luminescent Solar Concentrators. *Nano Energy* **2020**, *76*, No. 105039.

(27) Liu, X.; Luo, B.; Liu, J.; Jing, D.; Benetti, D.; Rosei, F. Eco-Friendly Quantum Dots for Liquid Luminescent Solar Concentrators. *J. Mater. Chem. A* **2020**, *8*, 1787−1798.

(28) Mateen, F.; Lee, S. Y.; Hong, S.-K. Luminescent Solar Concentrators Based on Thermally Activated Delayed Fluorescence Dyes. *J. Mater. Chem. A* **2020**, *8*, 3708−3716.

(29) Meinardi, F.; Ehrenberg, S.; Dhamo, L.; Carulli, F.; Mauri, M.; Bruni, F.; Simonutti, R.; Kortshagen, U.; Brovelli, S. Highly Efficient Luminescent Solar Concentrators Based on Earth-Abundant Indirect-Bandgap Silicon Quantum Dots. *Nat. Photonics* **2017**, *11*, 177−185.

(30) Imran, M.; Caligiuri, V.; Wang, M.; Goldoni, L.; Prato, M.; Krahne, R.; De Trizio, L.; Manna, L. Benzoyl Halides as Alternative Precursors for the Colloidal Synthesis of Lead-Based Halide Perovskite Nanocrystals. *J. Am. Chem. Soc.* **2018**, *140*, 2656−2664.

https://doi.org/10.1021/acsaem.1c01498
ACS Appl. Energy Mater. 2021, 4, 10565−10573

(31) Vybornyi, O.; Yakunin, S.; Kovalenko, M. V. Polar-Solvent-Free Colloidal Synthesis of Highly Luminescent Alkylammonium Lead Halide Perovskite Nanocrystals. *Nanoscale* **2016**, *8*, 6278−6283.
(32) Klimov, V. I.; Baker, T. A.; Lim, J.; Velizhanin, K. A.; McDaniel, H. Quality Factor of Luminescent Solar Concentrators and Practical Concentration Limits Attainable with Semiconductor Quantum Dots. *ACS Photonics* **2016**, *3*, 1138−1148.
(33) Coropceanu, I.; Bawendi, M. G. Core/Shell Quantum Dot Based Luminescent Solar Concentrators with Reduced Reabsorption and Enhanced Efficiency. *Nano Lett.* **2014**, *14*, 4097−4101.
(34) Guria, A. K.; Dutta, S. K.; Adhikari, S. D.; Pradhan, N. Doping Mn 2+ in Lead Halide Perovskite Nanocrystals: Successes and Challenges. *ACS Energy Lett.* **2017**, *2*, 1014−1021.
(35) Mir, W. J.; Jagadeeswararao, M.; Das, S.; Nag, A. Colloidal Mn-Doped Cesium Lead Halide Perovskite Nanoplatelets. *ACS Energy Lett.* **2017**, *2*, 537−543.
(36) Li, X.; Guo, Y.; Luo, B. Improved Stability and Photoluminescence Yield of Mn2+-Doped $CH_3NH_3PbCl_3$ Perovskite Nanocrystals. *Crystals* **2018**, *8*, 4.
(37) Arunkumar, P.; Gil, K. H.; Won, S.; Unithrattil, S.; Kim, Y. H.; Kim, H. J.; Im, W. Bin. Colloidal Organolead Halide Perovskite with a High Mn Solubility Limit: A Step Toward Pb-Free Luminescent Quantum Dots. *J. Phys. Chem. Lett.* **2017**, *8*, 4161−4166.
(38) Scardi, P.; Leoni, M.; Beyerlein, K. R. On the Modelling of the Powder Pattern from a Nanocrystalline Material. *Z. Kristallogr.* **2011**, *226*, 924−933.
(39) Wang, P.; Dong, B.; Cui, Z.; Gao, R.; Su, G.; Wang, W.; Cao, L. Synthesis and Characterization of Mn-Doped $CsPb(Cl/Br)_3$ Perovskite Nanocrystals with Controllable Dual-Color Emission. *RSC Adv.* **2018**, *8*, 1940−1947.
(40) Liu, H.; Wu, Z.; Shao, J.; Yao, D.; Gao, H.; Liu, Y.; Yu, W.; Zhang, H.; Yang, B. $CsPb_xMn_{1-x}Cl_3$ Perovskite Quantum Dots with High Mn Substitution Ratio. *ACS Nano* **2017**, *11*, 2239−2247.
(41) Chou, C.-H.; Hsu, M.-H.; Chen, F.-C. Flexible Luminescent Waveguiding Photovoltaics Exhibiting Strong Scattering Effects from the Dye Aggregation. *Nano Energy* **2015**, *15*, 729−736.
(42) Yang, C.; Liu, D.; Lunt, R. R. How to Accurately Report Transparent Luminescent Solar Concentrators. *Joule* **2019**, *3*, 2871−2876.
(43) Zhou, Y.; Benetti, D.; Fan, Z.; Zhao, H.; Ma, D.; Govorov, A. O.; Vomiero, A.; Rosei, F. Near Infrared, Highly Efficient Luminescent Solar Concentrators. *Adv. Energy Mater.* **2016**, *6*, No. 1501913.
(44) Liu, H.; Li, S.; Chen, W.; Wang, D.; Li, C.; Wu, D.; Hao, J.; Zhou, Z.; Wang, X.; Wang, K. Scattering Enhanced Quantum Dots Based Luminescent Solar Concentrators by Silica Microparticles. *Sol. Energy Mater. Sol. Cells* **2018**, *179*, 380−385.
(45) Debije, M. G.; Teunissen, J.-P.; Kastelijn, M. J.; Verbunt, P. P. C.; Bastiaansen, C. W. M. The Effect of a Scattering Layer on the Edge Output of a Luminescent Solar Concentrator. *Sol. Energy Mater. Sol. Cells* **2009**, *93*, 1345−1350.
(46) Portnoi, M.; Sol, C.; Tummeltshammer, C.; Papakonstantinou, I. Impact of Curvature on the Optimal Configuration of Flexible Luminescent Solar Concentrators. *Opt. Lett.* **2017**, *42*, 2695.

https://doi.org/10.1021/acsaem.1c01498
ACS Appl. Energy Mater. 2021, 4, 10565−10573